HOKKAIDO UNIVERSITY

Title	Determination of Source Parameters of Deep Earthquakes around Japan from Long-period Rayleigh Waves
Author(s)	SATAKE, Kenji
Citation	Journal of the Faculty of Science, Hokkaido University. Series 7, Geophysics, 7(4), 269-280
Issue Date	1984-02-29
Doc URL	https://hdl.handle.net/2115/8741
Type	departmental bulletin paper
File Information	7(4)_p269-280.pdf

Hokkaido University Collection of Scholarly and Academic Papers : HUSCAP

Jour. Fac. Sci., Hokkaido Univ., Ser. VII (Geophysics), Vol. 7, No. 4, 269-280, 1984.

Determination of Source Parameters of Deep Earthquakes around Japan from Long-period Rayleigh Waves

Kenji Satake

Department of Geophysics, Faculty of Science, Hokkaido University, Sapporo 060, Japan

(Received October 31, 1983)

Abstract

Source parameters of fifteen deep and intermediate earthquakes which occurred in and around Japan are determined. Focal mechanisms are obtained from first-motion data. The long-period Rayleigh waves recorded by IDA network are used for the determination of source process time τ and seismic moment M_0. It is found that M_0 is proportional to τ^3. Broad-band body wave magnitude and $\log M_0$ is linearly related. This relationship suggests that the apparent stress of deep and intermediate shocks is nearly constant for a wide range of depth.

1. Introduction

Systematic researches of the source process of deep and intermediate earthquakes (hereafter we collectively call them "deep earthquakes", unless otherwise mentioned) were not numerous, because of infrequent occurrence of deep events. The relationship among the source parameters such as seismic moment, source process time and magnitude was studied by a few investigators (Abe, 1982; Vassiliou and Kanamori, 1982). For most of the previous studies of deep events, body waves were used (e.g., Mikumo, 1971; Wyss and Molnar, 1972; Chung and Kanamori, 1980; Sasatani, 1980). A few studies employed long-period surface waves (Abe, 1972; Furumoto and Fukao, 1976; Osada and Abe, 1981). A weak excitation of fundamental mode surface waves by deep shocks has been a major reason of this small number of surface wave analyses of deep events. However, long-period surface waves represent the overall feature of earthquakes. Furthermore, surface wave analysis of deep events makes it possible to compare source parameters between deep and shallow earthquakes on a common basis, since surface wave analyses have been exten-

sively made for shallow events (e.g., Kanamori and Given, 1982).

In this paper source process times and seismic moments of deep shocks are determined from long-period Rayleigh waves recorded by IDA (International Deployment of Accelerographs) network (Agnew et al., 1976). Because of the long-period characteristics of IDA instruments, it is possible to analyze surface waves of deep events.

2. Earthquakes and mechanisms

Six deep ($h > 300$ km) and nine intermediate ($70 \leq h \leq 300$ km) earthquakes which occurred in and around Japan from 1977 to 1981 are selected. Figure 1 and Table 1 show their epicenters. All the events with magnitude M above 6.5 in JMA scale are included. Since M is not given by JMA for event No. 2, we adopt the value given by Utsu (1982). The long-period Rayleigh waves of events $M \geq 6.5$ are recorded with adequate signal-to-noise ratio by IDA network. Origin times (GMT), epicenters and depths in Table 1 are given by NEIS. The depth of event No. 9 is 69 km in Table 1. Because JMA gives 70 km for this event, it is included in this study.

Fault plane solutions are determined from the first-motion data given in ISC, EDR and JMA bulletins. Since the first-motions of deep events are clear

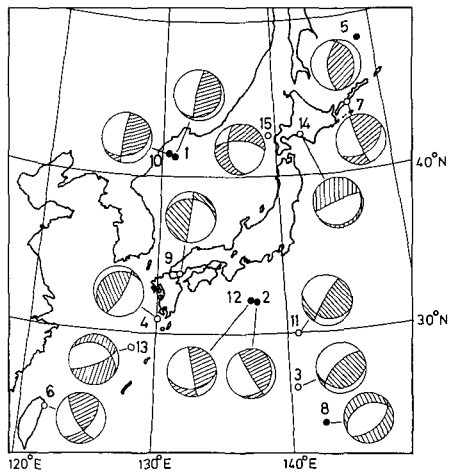

Fig. 1 Locations and mechanisms of earthquakes used. The epicenters for intermediate and deep events are shown by open and solid circles, respectively. Focal mechanisms are shown in equal-area projection of the lower hemisphere. Hatched area represents compressional quadrant.

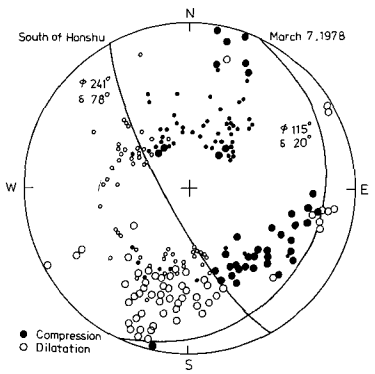

Fig. 2 Equal-area projection of the lower hemisphere for the first-motion data of the Honshu event (No. 2). The open and solid circles represent compression and dilatation, respectively. The large symbols are the readings from long-period seismograms, and the small symbols are from short-period seismograms. ϕ and δ denote dip direction and dip angle, respectively.

without contaminations of free-surface phases, bulletin reports are reliable. Furthermore, for deep events around Japan, the dense distribution of JMA stations enables us to determine two nodal planes almost uniquely. An example of the fault plane solutions is shown in Fig. 2 for the Honshu event (No. 2 of Table 1 and Fig. 1). 207 readings from bulletins are plotted. Two nodal planes are determined very well. The nodal plane solutions thus determined are given in Table 1. In the table ϕ and δ correspond to dip direction (measured clockwise from the north) and dip angle, respectively.

3. Surface wave analysis

Rayleigh wave seismograms recorded by IDA network are windowed between group velocities of 3.4 and 4.0 km/s. These values are not fixed but changed by up to 0.2 km/s according to visual inspections. This windowing separates fundamental Rayleigh waves from higher modes which are often excited by deep events. The seismograms thus windowed are Fourier transformed. All the phases R1-R5 are examined and as many phases as possible are analyzed.

First we determine source process time. For shallow earthquakes Kanamori and Given (1981) used an empirical relation between magnitude and source process time to correct the source finiteness. However, such an empirical relation is presently unknown for deep shocks. In this study source process time for individual shock is determined directly from surface wave spectra.

Trios of phases (e.g., R2, R3 and R4) observed at one station are used to cancel the propagation effect and the directional source phases (Furumoto and Nakanishi, 1983; Nakanishi and Kanamori, 1982). Averaging over many stations, we obtain the source process time τ. τ is determined at the period where the scatter is minimum for each event. This period ranges from 244 to 301 s in this study. The values of τ are given in Table 1 with standard deviations. Table 1 shows that standard errors of τ reach 20 s. Considering the fact that the sampling interval of IDA data used in this study is 20 s, we assume a step function point source (i.e. $\tau=0$ s) when the measured τ is less than 10 s.

Next we determine seismic moment using a method similar to that used by Kanamori and Given (1981). They determine the fault parameters and the seismic moment simultaneously using the moment tensor inversion while we obtain the fault parameters from first-motion data in this study. The basic equation is given by

$$AM_0 = Vr \tag{1}$$

where

$$A = s_R S_R^{(1)} + p_R P_R^{(1)} + iq_R Q_R^{(1)}. \tag{2}$$

s_R, p_R and q_R are determined from fault plane geometry and station azimuth (Kanamori and Stewart, 1976). $P_R^{(1)}$, $Q_R^{(1)}$ and $S_R^{(1)}$ are Rayleigh wave excitation functions calculated for a given Earth model. M_0 is the scalar seismic moment. Vr is the Fourier transform of the observed seismograms corrected for geometrical spreading, propagation, source process time and polar phase shifts. Expression of Vr is given by Kanamori and Given (1981). For the propagation corrections, the values of Q, group velocities and phase velocities compiled by Dziewonski and Anderson (1981) are used in this study. Excitation functions are calculated for the Earth model 5.08 M (Kanamori, 1970). We determine M_0 for each phase (R1 to R5) at all the stations. We average the values from all the phases and the stations to obtain a value of M_0 for a given period. In Eq. (1), a step function point source is assumed. For large events the corrections for the source finiteness and the finite rise time are neccessary. Since the details of the rupture mode are unknown, we assume that the overall source finiteness effect is given by

$$\frac{\sin(\pi\tau/T)}{(\pi\tau/T)}\exp(-i\pi\tau/T), \tag{3}$$

where T is the wave period and τ is the source process time which has already been determined. The left hand side of Eq. (1) must be multiplied by Eq. (3) to correct the finiteness.

The amplitude and phase of Vr at a period of 256 s for the Honshu event

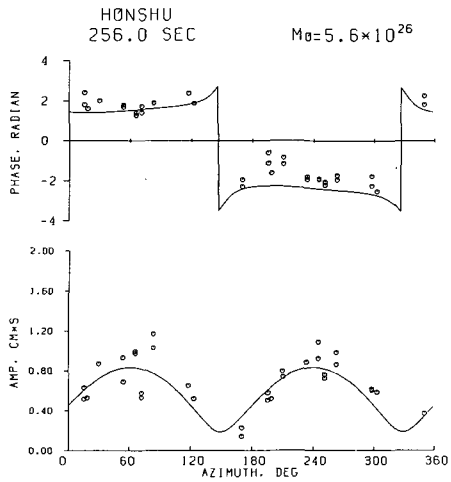

Fig. 3 Amplitude and phase spectra at a period of 256 s for event No. 2 as a function of azimuth. The azimuth is measured clockwise from the north. Two measurements at the same azimuth are obtained from multiple phases such as R2 and R4.

(No. 2) are shown in Fig. 3 as a function of azimuth. Figure 3 also shows the synthetic spectra (l.h.s. of Eq. (1)) of $M_0=5.6\times10^{26}$ dyne • cm corrected for the finiteness. Although the phase spectrum is not neccessary for the determination of M_0, comparison of synthetic and observed radiation patterns makes it possible to check the agreement of the surface wave mechanism and the mechanism determined by first-motion data. Systematic deviations of the observed spectra from the synthetic radiation patterns for a particular azimuth indicate the existence of lateral heterogeneity of the phase velocity and Q structure. These discrepancies cannot be reduced as long as we use a laterally homogeneous Earth model for the propagation corrections.

Analyses are made at four different periods. They are, 150, 197, 256 and 300 s. Figure 4 shows the values of M_0 of four events as a function of period. In this period range ($150\leq T\leq300$ s), M_0 is found to be nearly constant. Equation (3) shows that large τ relative to T causes a significant effect of finiteness. For example, the Kunashiri event (No. 7) in Fig. 4 has a source process time of 66 s. If we assume $\tau=0$ s, then we underestimate the values of M_0 by 10 to 30%.

For two events (Nos. 3 and 10), some of the fault parameters cannot be determined from the first-motion data alone. We adopt a method similar to that of Weidner and Aki (1973), in which we change the undetermined parameters iteratively. We regard a parameter value as the best fit, when it gives the

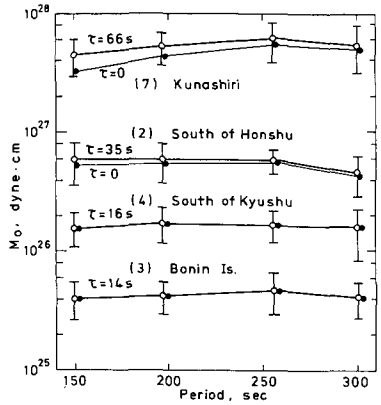

Fig. 4 Seismic moments of four events as a function of period. Open symbols with error bars represent the seismic moments corrected for the finiteness. The uncorrected values are shown by solid symbols.

minimum of RMS residual (observed minus calculated) of amplitude and phase.

4. Seismic moment, source process time and magnitude

The seismic moments and source process times determined in this study are summarized in Table 1 with their standard deviations. The number of trios used for the determination of τ is 3 to 15. M_0 is the averaged value over the four periods. For each period, 13 to 37 phases of various stations are used. Standard deviation of M_0 ranges 28 to 67% of M_0. For some of the events, other investigators independently obtained the seismic moments. Silver and Jordan (1983) obtained the total moment and the characteristic source time for events Nos. 2 and 7. Their values are very similar to our estimates of seismic moment and source process time. On the basis of GDSN (Global Digital Seismic Network) data, Dziewonski et al. (1981) and Dziewonski and Woodhouse (1983) obtained the moment tensor solutions for events Nos. 2, 3, 6, 13, 14 and 15. They mainly used body wave parts of seismograms and obtained almost the same values as our estimates. The differences are less than 30% of M_0 for most of the events.

The relation between source process time and seismic moment is shown in Fig. 5. The source process time of a deep shock which occurred around Japan and determined by Furumoto and Nakanishi (1983) is added to our data. They found that source process times for large deep shocks are roughly constant in a narrow range of seismic moment (10^{27}-10^{28} dyne • cm). We extend the range

Table 1 List of earthquakes

No.	Yr.	Date (m d)	Time (h m s)	Lat. (°N)	Long. (°E)	Depth (km)	Magnitudes m_1 M_{JMA} m_B m_W	Mechanism (ϕ δ) (ϕ δ)	M_0 ΔM_0 (10^{25}dyn • cm)	τ $\Delta\tau$ (sec)	σ_a (bar)
1	1977	3 9	14 27 53.6	41.61	130.88	528	5.9 7.2 6.7 6.8	143 17 287 76	25 8.1	0 0	30
2	1978	3 7	2 48 47.6	32.01	137.61	439	6.9 7.6 6.9 6.9	115 20 241 78	56 18	35 12	46
3	1978	3 15	22 4 40.1	26.42	140.56	263	6.1 6.7 6.7 6.5	166 22 320 70	4.2 1.6	14 19	191
4	1978	5 23	7 50 28.2	31.06	130.14	161	6.3 6.7 6.5 6.7	123 74 323 17	16 6.0	16 12	16
5	1978	6 21	11 10 38.2	48.31	148.61	377	5.9 6.7 6.4 6.5	65 30 268 62	5.4 2.8	23 18	29
6	1978	9 2	1 57 33.4	24.90	121.99	109	6.1 6.5 6.4 6.5	135 50 241 72	4.4 2.9	0 0	36
7	1978	12 6	14 2 1.0	44.59	146.58	91	6.7 7.7 7.5 7.3	147 41 245 83	534 215	66 3	126
8	1979	5 18	20 18 1.1	24.13	142.40	567	5.8 6.6 6.6 6.5	134 49 329 42	6.0 1.7	0 0	69
9	1979	7 13	8 10 11.7	33.84	131.80	69	5.9 6.1 6.2 6.4	8 24 98 90	3.0 1.4	0 0	15
10	1979	8 16	21 31 26.3	41.81	130.79	588	6.1 6.8 6.7 6.7	161 28 275 78	17 6.4	29 19	48
11	1979	12 11	17 26 16.8	28.88	140.70	110	6.1 6.7 6.7 6.7	192 30 300 80	18 12	36 21	38
12	1980	4 22	5 34 13.8	32.11	137.57	394	5.7 6.6 6.6 6.6	80 90 170 35	7.0 2.3	12 15	69
13	1981	1 2	15 39 47.3	29.24	128.14	242	6.1 6.7 6.9 6.9	35 31 162 70	38 16	31 14	58
14	1981	1 23	4 58 31.5	42.52	142.12	116	6.3 7.1 6.8 6.8	148 10 337 80	26 14	31 7	53
15	1981	5 8	23 34 44.9	42.66	139.13	200	6.0 6.4 6.4 6.5	7 60 250 52	6.0 2.0	0 0	23

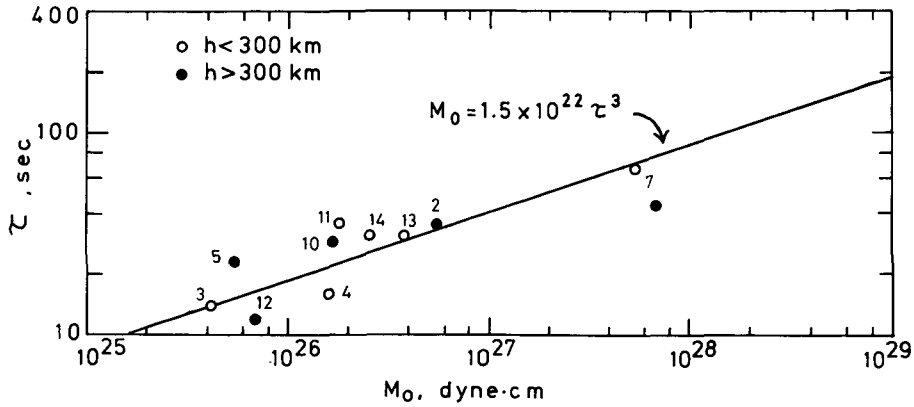

Fig. 5 The relation between seismic moment and source process time. Open and solid symbols represent intermediate and deep earthquakes, respectively. The numbers attached to symbols correspond to the event number in Table 1. A deep earthquake studied by Furumoto and Nakanishi (1983) is added. Equation (4) in the text is also shown by a solid line.

down to 10^{25} dyne • cm. Figure 5 shows a tendency that smaller shocks have shorter source process times. Assuming a slope of 1/3 from the figure, we fit a straight line to these data in a least-squares sense, that is

$$M_0=1.5\times10^{22}\tau^3. \quad (4)$$

This relation is shown by a solid line in Fig. 5. Equation (4) is very close to the relation for low angle thrust earthquakes along trenches obtained by Furumoto and Nakanishi (1983).

Four kinds of magnitudes are listed in Table 1. m_1 is the body wave magnitude given by NEIS. Since it is determined from short-period (usually 1 s) P waves, we call it m_1 instead of m_b in this paper. m_1 represents the size of an earthquake at its beginning (Kanamori, 1983). M_{JMA} is magnitude given by JMA. This scale is based on relatively long-period ($T \leq 5$ s) waves. Since M_{JMA} is assigned to only Japanese events, it is impossible to compare with other data. To overcome these inconveniences, we employed the broad-band body wave magnitude m_B, which is determined from amplitudes and periods of body waves on various types of seismograms (e.g., Abe and Kanamori, 1979). In this study the amplitudes and periods of P, PP and S waves recorded at Pasadena are mainly used. Long-period ($T \geq 3$ s) reports in EDR are supplementarily used. The average period of body waves ranges 2 to 11 s. These periods are long enough to represent the overall size of earthquakes. The values of m_B and M_0 are plotted in Fig. 6. Although the data are not equally distributed, a linear relation between m_B and log M_0 is seen in this figure. A similar plot was given

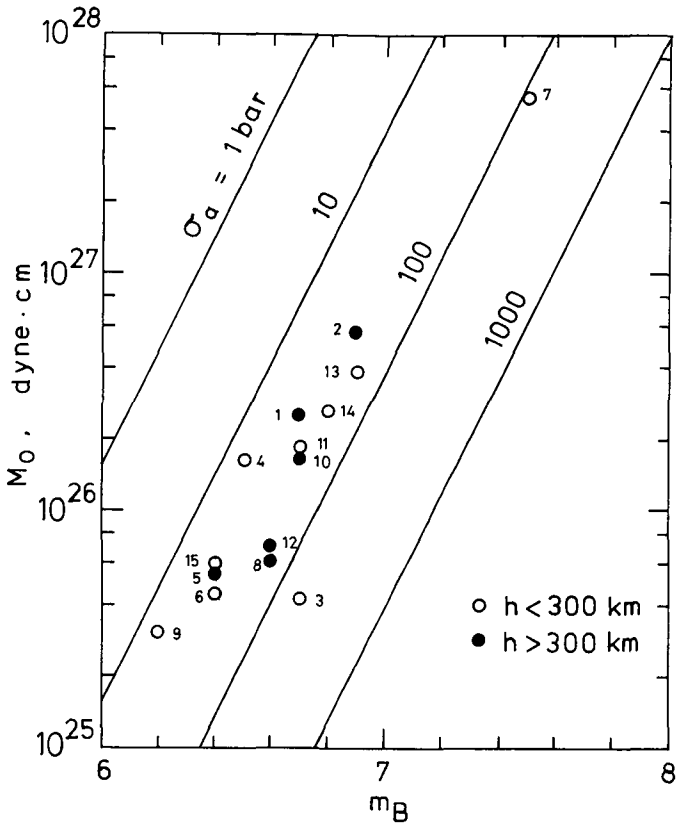

Fig. 6 The relation between body wave magnitude and seismic moment. Open and solid symbols represent intermediate and deep earthquakes, respectively. The numbers attached to symbols correspond to the event number in Table 1. The straight lines represent constant apparent stress.

by Abe (1982) for a different set of worldwide data. On the basis of this linear relationship between m_B and log M_0, Kanamori (1983) introduced a moment magnitude scale m_W for deep events. The values of m_W that are calculated from M_0 are listed in Table 1. Since the comparison of m_B and m_W is essentially the same as of m_B and log M_0, m_B and m_W agree very well (Table 1).

5. Discussion

For low angle thrust earthquakes along trenches, Furumoto and Nakanishi (1983) obtained a formula similar to Eq. (4). Assuming a constant stress drop and rupture velocity, they derived a scaling relation based on that formula. On

the other hand, it is suggested that stress drop increases with increasing depth for deep earthquakes (Mikumo, 1971 ; Sasatani, 1980). If this is the case, the scaling relation cannot be applied to deep earthquakes.

The relation between m_B and M_0 is discussed by Abe (1982). Combining the Gutenberg-Richter's magnitude-energy relation and the definition of the apparent stress σ_a, he obtained

$$\log M_0 = 2.4 m_B + 5.8 - \log(\sigma_a/\mu), \tag{5}$$

where μ is the rigidity near the source. Equation (5) means that m_B and $\log M_0$ are linearly related if the apparent stress is constant. Assuming $\mu = 9 \times 10^{11}$ dyne/cm^2 as the average for the depth range considered here, the relations for $\sigma_a = 1$, 10, 100 and 1000 bar are shown in Fig. 6. It is seen in this figure that most of the earthquakes have σ_a between 10 and 100 bar. Each value of σ_a is summarized in Table 1 and the average is 56 bar. If we change μ as a function of depth, we have similar values of σ_a. Figure 6 suggests that the apparent stress is nearly constant over a wide range of depth. Abe (1982) obtained the same result from the worldwide data, which were obtained by various methods and types of waves. In this study the region is limited to Japan and its vicinity, and seismic moments and magnitudes are determined by the same method for all the events. In spite of the differences in region and analysis method, the constant apparent stress is obtained for both data-sets, Abe (1982) and this study.

6. Conclusion

The seismic moment M_0 and the source process time τ of 15 deep earthquakes ($6.2 \leq m_B \leq 7.5$) which occurred in and around Japan are determined from the analysis of surface waves recorded by IDA network. It is found that M_0 is proportional to τ^3. A linear relationship between $\log M_0$ and m_B suggests the apparent stress is nearly constant over a wide range of depth.

Acknowledgements

I am grateful to Prof. Katsuyuki Abe for valuable suggestions and critical review of the manuscript. I thank Dr. Ichiro Nakanishi for reading the manuscript, Dr. Muneyoshi Furumoto for preprint.

The IDA data used in this study were made available by courtesy of the IDA project team at the Institute of Geophysics and Planetary Physics, University of California, San Diego.

The computations were made at the Hokkaido University Computing Center.

References

Abe, K., 1972. Focal process of the South Sandwich Islands earthquake of May 26, 1964. Phys. Earth Planet. Inter., **5**, 110-122.

Abe, K., 1982. Magnitude, seismic moment and apparent stress for major deep earthquakes. J. Phys. Earth, **30**, 321-330.

Abe, K. and H. Kanamori, 1979. Temporal variation of the activity of intermediate and deep focus earthquakes. J. Geophys. Res., **84**, 3589-3595.

Agnew, D., J. Berger, R. Buland, W. Farrell and F. Gilbert, 1976. International deployment of accelerometers: A network for very long period seismology, EOS. Trans. Am. Geophys. Union, **57**, 180-188.

Chung, W.-Y. and H. Kanamori, 1980. Variation of seismic source parameters and stress drops within a descending slab and its implications in plate mechanics. Phys. Earth Planet. Inter., **23**, 134-159.

Dziewonski, A.M. and D.L. Anderson, 1981. Preliminary reference Earth model. Phys. Earth Planet. Inter., **25**, 297-356.

Dziewonski, A.M., T.-A. Chou and J.H. Woodhouse, 1981. Determination of earthquake source parameters from waveform data for studies of global and regional seismicity. J. Geophys. Res., **86**, 2825-2852.

Dziewonski, A.M. and J.H. Woodhouse, 1983. An experiment in systematic study of global seismicity: Centroid-moment tensor solutions for 201 moderate and large earthquakes of 1981. J. Geophys. Res., **88**, 3247-3271.

Furumoto, M. and Y. Fukao, 1976. Seismic moment of great deep shocks. Phys. Earth Planet. Inter., **11**, 352-357.

Furumoto, M. and I. Nakanishi, 1983. Source times and scaling relations of large earthquakes. J. Geophys. Res., **88**, 2191-2198.

Kanamori, H., 1970. Velocity and Q of mantle waves. Phys. Earth Planet. Inter., **2**, 259-275.

Kanamori, H., 1983. Magnitude scale and quantification of earthquakes. Tectonophys., **93**, 185-199.

Kanamori, H. and J.W. Given, 1981. Use of long-period surface waves for rapid determination of earthquake-source parameters. Phys. Earth Planet. Inter., **27**, 8-31.

Kanamori, H. and J.W. Given, 1982. Use of long-period surface waves for rapid determination of earthquake source parameters: 2. Preliminary determination of source mechanisms of large earthquakes ($Ms \geq 6.5$) in 1980. Phys. Earth Planet. Inter., **30**, 260-268.

Kanamori, H. and G.S. Stewart, 1976. Mode of the strain release along the Gibbs fracture zone, Mid-Atlantic ridge. Phys. Earth Planet. Inter., **11**, 312-332.

Mikumo, T., 1971. Source process of deep and intermediate earthquakes as inferred from long-period P and S waveforms 2. Deep-focus and intermediate-depth earthquakes around Japan. J. Phys. Earth, **19**, 303-320.

Nakanishi, I. and H. Kanamori, 1982. Effects of lateral heterogeneity and source process time on the linear moment tensor inversion of long-period Rayleigh waves. Bull. Seism. Soc. Am., **72**, 2063-2080.

Osada, M. and K. Abe, 1981. Mechanism and tectonic implications of the great Banda Sea earthquake of November 4, 1963. Phys. Earth Planet. Inter., **25**, 129-139.

Sasatani, T., 1980. Source parameters and rupture mechanism of deep-focus earthquakes. J.

Fac. Sci. Hokkaido Univ., Ser. 7 (Geophys.), **6**, 301-384.
Silver, P.G. and T.H. Jordan, 1983. Total-moment spectra of fourteen large earthquakes. J. Geophys. Res., **88**, 3273-3293.
Utsu, T, 1982. Catalog of large earthquakes in the region of Japan from 1885 through 1980. Bull. Earthq. Res. Inst., Tokyo Univ., **57**, 401-463 (in Japanese).
Vassiliou, M.S. and H. Kanamori, 1982. The energy release in earthquakes. Bull. Seism. Soc. Am., **72**, 371-387.
Weidner, D.J. and K. Aki, 1973. Focal depth and mechanism of mid-ocean ridge earthquakes. J. Geophys. Res., **78**, 1818-1831.
Wyss, M. and P. Molnar, 1972. Source parameters of intermediate and deep focus earthquakes in the Tonga arc. Phys. Earth Planet. Inter., **6**, 279-292.